ADVANCED OPTICAL MATERIALS
www.advopticalmat.de

High Quality Factor Microcavity for Van der Waals Semiconductor Polaritons Using a Transferrable Mirror

*Eunice Y. Paik, Long Zhang, Shaocong Hou, Haonan Zhao, Yu-Hsun Chou, Stephen R. Forrest, and Hui Deng**

Semiconductor microcavities with a high quality-factor are an important component for photonics research and technology, especially in the strong coupling regime. While van der Waals semiconductors have emerged as an interesting platform for photonics due to their strong exciton–photon interaction strength and engineering flexibility, incorporating them in photonic devices requires heterogeneous integration and remains a challenge. This study demonstrates a method to assemble high quality factor microcavities for van der Waals materials, using high reflectance top mirrors which, similar to van der Waals materials themselves, can be nondestructively and reliably peeled off the substrate and transferred onto the rest of the device. Microcavities are created with quality factors consistently above 2000 and up to 11000 ± 800; and the strong coupling regime is demonstrated. The method can be generalized to other types of heterogeneously integrated photonic structures and will facilitate research on cavity quantum electrodynamic and photonic systems using van der Waals materials.

1. Introduction

Optical microcavities are a powerful tool for exploring cavity quantum electrodynamics (QED) phenomena, controlling quantum information systems, and engineering photonic devices. They tightly confine light in at least one dimension, and thus can strongly modify the interactions between light and matter within the cavity. In microcavities with high quality factors (Q-factors), when the light–matter coupling in the cavity becomes stronger than the loss and decoherence of the cavity or the medium, the cavity effect is no longer perturbative, and new light and matter hybrid eigenmodes, polaritons, are formed.[1–3]

A challenge in the use of microcavities is to nondestructively integrate the active media without introducing excessive defects and impurities. The challenge is especially pronounced for reaching the strong coupling regime. Consequently, with conventional materials such as group III–V and II–IV semiconductors, polariton systems often require monolithically grown structures consisting of tall stacks of distributed Bragg reflectors (DBRs) and embedded quantum well layers, all closely latticed-matched. These devices are bulky and demanding to fabricate. Polaritons have been achieved in only a handful of materials, mostly operating at low temperatures.

In recent years, van der Waals (vdW) materials, such as transition metal dichalcogenides (TMDs), have emerged as a new type of optical media. They possess many special properties including excitons and polaritons that are stable at the room temperature.[4–8] Contrary to conventional materials, TMDs can be integrated with a variety of substrates and cavity configurations, albeit heterogeneous integration is required. Among the demonstrated polariton systems, a closed planar Fabry–Perót cavity continues to be one of the most versatile, for it has a

E. Y. Paik, L. Zhang, H. Zhao, H. Deng
Department of Physics
University of Michigan
Ann Arbor, Michigan 48109-2122, USA
E-mail: dengh@umich.edu

L. Zhang
Department of Physics
Xiamen University
Xiamen 361000, China

The ORCID identification number(s) for the author(s) of this article can be found under https://doi.org/10.1002/adom.202201440.

DOI: 10.1002/adom.202201440

S. Hou
School of Electrical Engineering and Automation
Wuhan University
Wuhan 430000, China

S. Hou
Department of Electrical and Computer Engineering
University of Michigan
Ann Arbor, Michigan 48109, USA

Y.-H. Chou
Department of Photonics
National Cheng Kung University
Tainan City 70101, Taiwan

S. R. Forrest
Departments of Electrical and Computer Engineering
Physics, and Materials Science and Engineering
University of Michigan
Ann Arbor, Michigan 48109, USA

robust structure with relatively simple cavity modes that are easy to model and measure. To create a Fabry–Perót cavity, the TMDs are transferred to the bottom half of the cavity and then enclosed by a top mirror. The top mirror can be created by direct deposition over the TMDs,[4,9] which requires high processing temperatures and chemical reactions, potentially introducing strain, impurity, and defects to the TMDs and affecting its optical quality. A second method is to use an open cavity system,[5,10] where the top mirror is mounted separately and then brought close to the sample by a piezo controlled stage. Such open cavities allow tuning of the cavity length, but it involves complex experimental setups and bulky equipment. A third method is to break off a piece of a SiO_2/TiO_2 DBR from its substrate and then directly place it on the TMDs.[11,12] Yet, traditional dielectric DBRs have strong bonds with the substrate, and thus they only break off under high impact force and randomly. It can be very difficult to find a sufficiently large and clean piece for subsequent integration.

In this work, we present a method to reliably create high-Q microcavities for vdW materials, using a transferrable DBR that is bonded to the substrate also by the vdW force. We show that the DBR, made of zinc sulfide (ZnS) and magnesium fluoride (MgF_2), can be readily exfoliated and transferred mechanically, enabling reliable creation of high-Q microcavities for vdW materials. Typical Q-factors are well above 2000 with the highest reaching 11000 ± 800. These vdW-material microcavities are resistant against degradation and allow control of the cavity detuning by changing the effective cavity length. Strong coupling is observed by measuring the anti-crossing of the upper and lower polariton modes in angle-resolved microphotoluminescence (PL) and reflection spectra. These results establish a reproducible, high-Q, vdW material exciton–polariton system for observing many body physics phenomena and developing polariton devices. The method is also applicable to other materials that require heterogeneously integrated photonic structures.

2. Results

2.1. Fabrication of vdW Material Microcavity with a Transferrable DBR

A schematic of the vdW material microcavity is shown in **Figure 1**a. It consists of a bottom DBR, a top DBR, and an encapsulated monolayer placed at the cavity field maximum. Each of the three parts are fabricated and characterized independently, then assembled via exfoliation and dry transfer as illustrated in Figure1b–i, enabling fast and reliable sample production.

The key to making such a cavity is to have a reproducible, high reflectance top-DBR that can be dry transferred onto the vdW material sample stack. This is achieved with a ZnS/MgF_2 DBR[13,14] fabricated via vacuum thermal evaporation (VTE) on a glass substrate. The VTE process results in a rela-

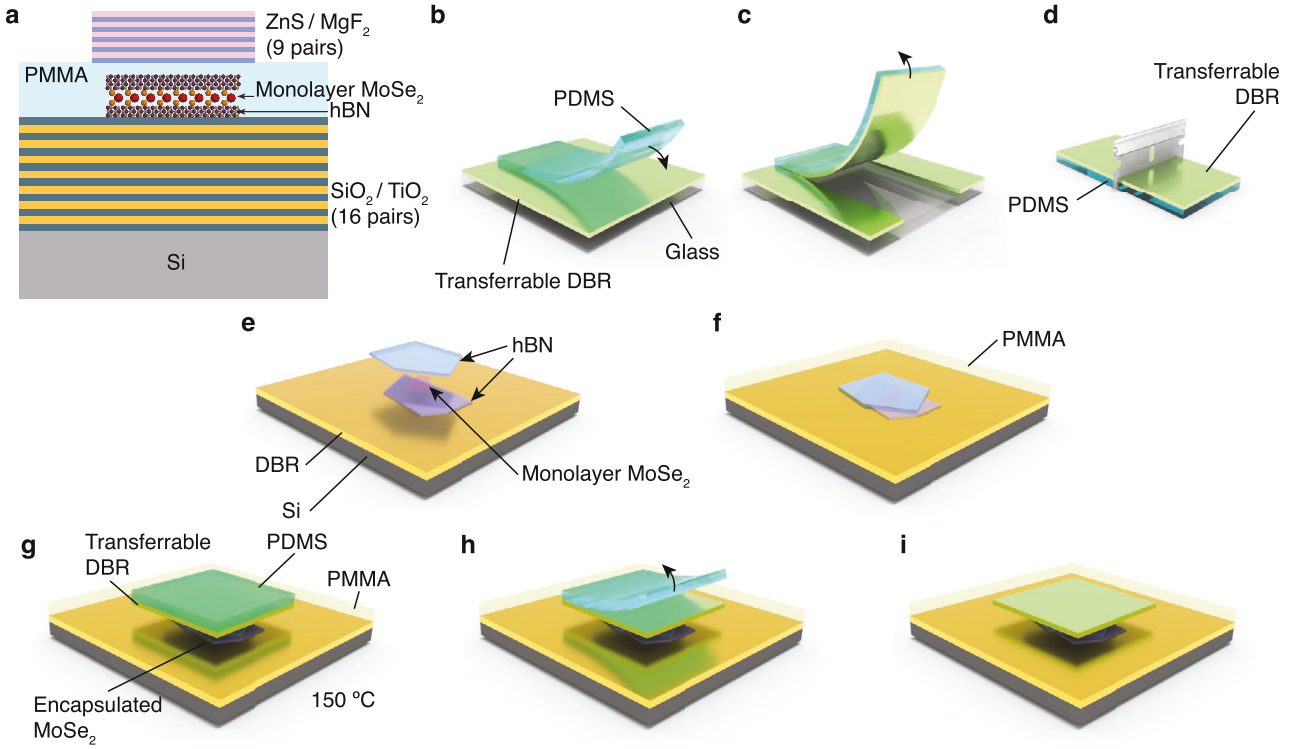

Figure 1. Cavity design and fabrication. a) Schematic of the polariton device consisting of a SiO_2/TiO_2 bottom DBR, hBN encapsulated monolayer $MoSe_2$, PMMA spacer layer, and a ZnS/MgF_2 top DBR. b–d) ZnS/MgF_2 DBR exfoliation procedure. b) PDMS sheet is brought into contact with the transferrable top DBR on a glass substrate. c) The PDMS sheet is lifted to peel off a segment of the top DBR. d) The peeled off top DBR is cut into a small piece. e–i) Sample fabrication procedure. e) hBN encapsulated $MoSe_2$ sample is stacked on top of the bottom DBR. f) PMMA is spin-coated on top of the encapsulated $MoSe_2$ sample. g) A small piece of top DBR is placed on top of the encapsulated $MoSe_2$ sample and heated to 150 °C. h) The PDMS layer is peeled off and the top DBR adheres to the PMMA. i) Image of the completed sample.

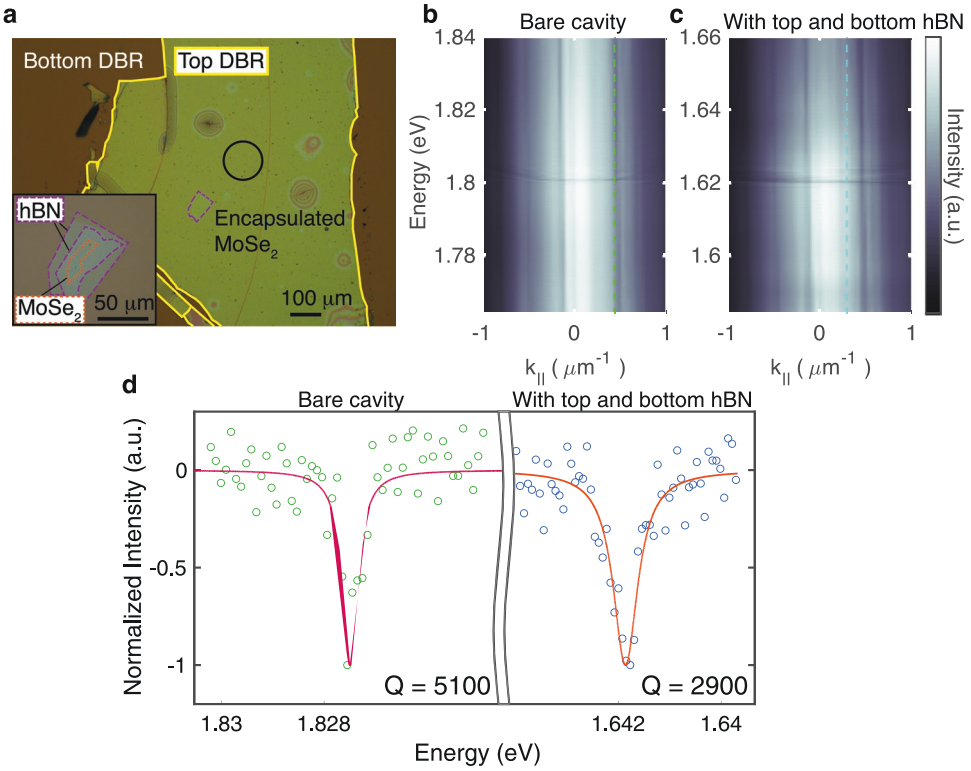

Figure 2. Cavity characterization. a) Optical image of the sample. The yellow solid line outlines the transferrable top DBR. The purple dashed line outlines the encapsulated $MoSe_2$ sample. The black circle indicates a clean bare cavity region for reflection characterization measurements. Inset: closeup image of the encapsulated $MoSe_2$ sample. The purple dashed lines outline the hBN layers. The orange dotted line outlines the monolayer $MoSe_2$. b) Angle-resolved reflection spectrum of the bare cavity region of the sample. Dashed green line marks the k value of the line-cut plot shown in (d). c) Angle-resolved reflection spectrum of the cavity with top and bottom hBN. Dashed blue line marks the *k* value of the line-cut plot shown in (d). d) Fitted cavity modes. The pink and orange solid lines indicate a Lorentzian fitting of the reflection spectrum line-cut. In order to improve the accuracy, we used a weighted fit, with weights of $\sqrt{|y - y_0|}$, where y_0 is the data offset.

tively weak van der Waals bonding between the DBR and the glass substrate, allowing it to be readily exfoliated. Moreover, ZnS and MgF_2 have both a high index contrast, 2.35 and 1.38 respectively, and low absorption in the visible to near-infrared range. Therefore a broadband and high reflectance mirror can be formed with only a few pairs of alternating quarter-wavelength thick layers of ZnS and MgF_2, with a total thickness of less than a micron. The thinness of the DBR also facilitates exfoliation.

In this work, we use a DBR stack comprising nine pairs of 40 nm ZnS/78 nm MgF_2 films. The fabrication parameters are carefully calibrated and controlled to ensure a clean, uniform film with high reflectivity. The full DBR is then exfoliated from the glass substrate using a polydimethylsiloxane (PDMS) handle, and can be cut into small pieces of desired areas of cavity coverage (Figure 1b–d).

To assemble the full cavity, we use a traditional bottom DBR comprised of 16 pairs of silicon dioxide (SiO_2) and titanium dioxide (TiO_2) with a 750 nm center wavelength. This DBR has a $\lambda/4$ SiO_2 spacer layer on top. The hBN encapsulated $MoSe_2$ was transferred on top of the bottom DBR using a dry transfer technique (Figure 1e). Polymethyl methacrylate (PMMA) with a molecular weight of 950K, diluted in 2% anisole (A2) was spun on top of the sample to control the cavity length (Figure 1f). Then, the top DBR was transferred on top of the encapsulated sample stack (Figure 1g). The PDMS handle was lifted off while the top DBR is now attached to the PMMA and sample stack (Figure 1h–i). The cavity resonance can be controlled via the hBN and PMMA thickness during the fabrication as discussed further in Section 2.2. **Figure 2**a is a top-down optical image of a complete cavity device. Note that the introduction of dust and cracking of the top DBR during the transfer process is unavoidable, but can be mitigated by sample cleaning, choosing clean 2D material layers, and performing the transfer in a glovebox.

2.2. Cavity Quality Factor, Resonance Control, and Reproducibility

Two of the most important properties of a cavity are its Q-factor and resonance energy. To characterize these properties, we perform angle-resolved reflection measurements using a supercontinuum white light source.

The Q-factor depends mainly on the reflectivity, absorption and scattering loss in the DBR and cavity layers. Taking the example shown in Figure 2a, we first focus on the bare cavity that consists of the top and bottom DBR and the PMMA spacer layer without the vdW material stack, as marked by the black circle. Its angle-resolved reflection spectrum and an example

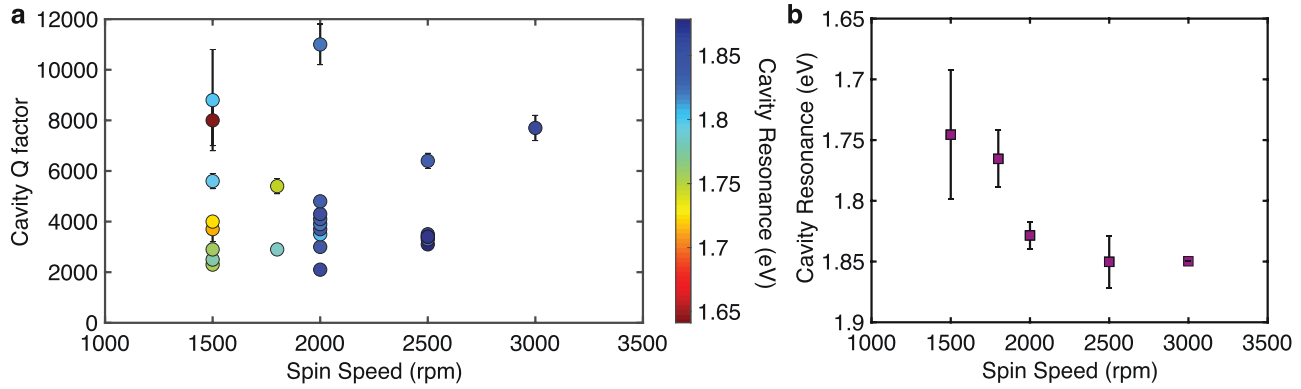

Figure 3. Systematic cavity characterization. a) A range of achievable cavity Q-factors and resonances with different PMMA spin speeds. The color bar indicates the cavity resonance energy. b) Cavity resonance wavelength versus PMMA spin speed. The error bars correspond to the standard deviation of the cavity resonance energy.

line cut are shown in Figure 2b,d. The line cut is fit by a Lorentzian line shape with a linewidth of 0.35 ± 0.02 meV, corresponding to a Q = 5100 ± 300. We then measure the region with both top and bottom hBN layers but not enclosing the monolayer of $MoSe_2$. As shown in Figure 2c,d, the introduction of hBN leads to a red-shift of the cavity resonance energy and lowers the Q-factor due to increased inhomogeneity in the sample introduced during the transfer processes of the 2D material layers and the top DBR. The relatively low reflection contrast of the cavity mode is due to the mismatch of the top and bottom DBR reflectivities.

To test the reliability of our fabrication methods, we performed a systematic characterization of the Q-factors and cavity resonance energies of 26 samples created with different PMMA spin speeds, as summarized in **Figure 3**a,b. We can reliably reach a Q-factor greater than 2000 for all 26 samples, and up to 11000 ± 800, with a median of 3700, comparable to the highest reported for vdW material cavities. There is no statistically significant dependence of the Q-factor on the PMMA spin speed within our sample set.

The cavity resonance energy in our device can be controlled by the combined top and bottom hBN and PMMA thicknesses. The hBN thickness can be precisely determined in the exfoliation step. Then the desired PMMA thickness can be controlled by the PMMA spin speed. As shown Figure 3b, higher PMMA spin speed leads to a thinner PMMA thickness and thereby a higher cavity resonance energy. For the 26 samples, a spin speed of 1500 rpm to 3500 rpm results in about 100 meV tuning in the resonance energy. Generally better reproducibility is obtained at higher spin speeds due to improved uniformity of the PMMA film thickness. For our devices, 2000 rpm is the optimal spin speed for maximum reproducibility, with the standard deviation of cavity resonance energy being 11 meV.

2.3. Strong Coupling

Our cavities feature high-Q, small mode-volume, and controllable matching between the exciton and cavity resonances. These properties are especially important for achieving strong coupling and performing exciton–polariton studies.

In the weak coupling regime, the hBN-$MoSe_2$-hBN cavity mainly modifies the exciton emission rate. To reach the strong coupling regime, the exciton–photon energy exchange rate needs to be enhanced by cavity confinement of near-resonant photon modes to overcome the exciton and photon decay or decoherence rates. When the strong coupling regime is established, coherent superposition of exciton and photon states leads to two new eigenstates, the lower and upper polaritons, with anti-crossing of the two separate resonances. The minimum separation, known as the vacuum Rabi splitting $E_{UP} - E_{LP} = 2\hbar\Omega$, corresponds to where the exciton and photon are in resonance. The condition of strong coupling is therefore

$$4\hbar\Omega > \gamma_{cav} + \gamma_{exc} \quad (1)$$

where γ_{cav} (γ_{exc}) is the full width half maximum linewidth of the cavity (exciton).

For our device, we measure the cavity resonance and linewidth via angle-resolved reflectance at the region of the sample with top and bottom hBN but without the monolayer, and we measure the exciton energy and photoluminescence (PL) linewidth before capping the sample stack with the top DBR. In the example shown in **Figure 4**, the cavity resonance energy at $k = 0$ is 1.646 eV and the exciton energy is 1.651 eV. The linewidths are γ_{cav} = 0.6 meV, which corresponds to Q = 2700, and γ_{exc} = 6.5 meV.

We characterize the $MoSe_2$ exciton–polaritons using both angle-resolved reflectance (Figure 4a,b) and micro-PL (Figure 4c,d) at 5K. Figure 4a shows the angle-resolved reflection and its corresponding linecut in Figure 4b. The upper and lower polariton dispersions are visible by the reflection dips in the spectrum. The reflection and PL energies of the upper and lower polariton dispersions match. By fitting a Gaussian line shape to the PL data, we extracted the upper and lower polariton energies and the trion energy. To determine the vacuum Rabi splitting $2\hbar\Omega$, we fit the polariton energies with

$$E_{LP,UP} = \frac{1}{2}\left[E_{exc} + E_{cav} + i(\gamma_{cav} + \gamma_{exc})\right] \pm \sqrt{4\hbar^2\Omega^2 + \left[E_{exc} - E_{cav} + i(\gamma_{cav} - \gamma_{exc})\right]^2} \quad (2)$$

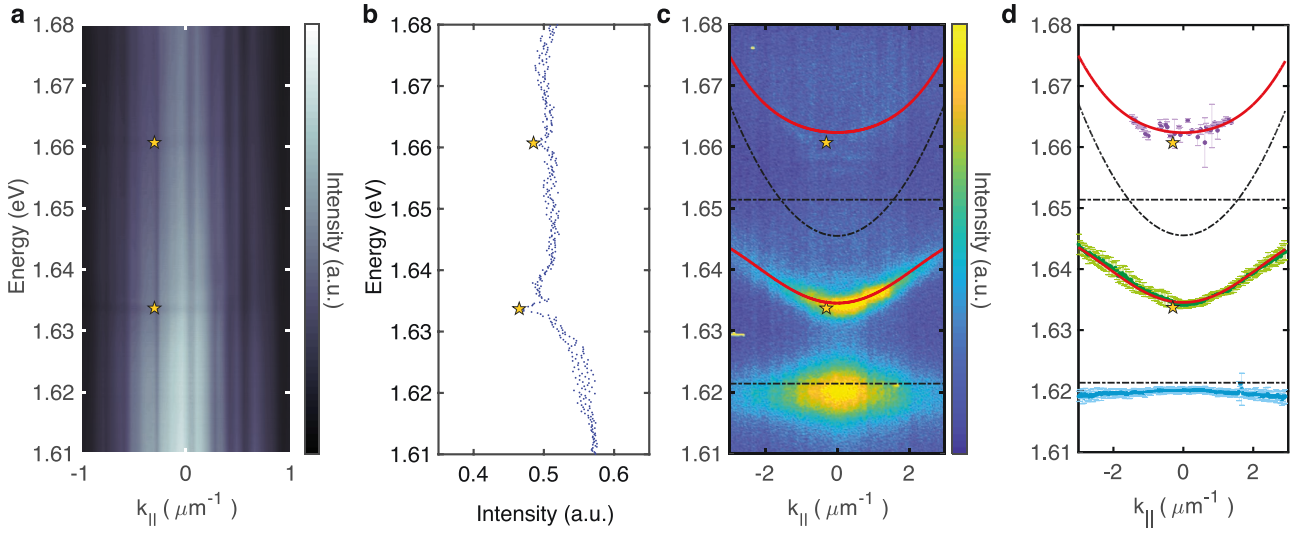

Figure 4. Spectral properties of the strongly coupled monolayer $MoSe_2$ polariton device. a) Angle-resolved reflection spectrum of the polariton device. The orange star indicates the location of the dip in the reflection spectrum at a given value of k. b) Line-cut of (a) at $k = -0.3$. c) Angle-resolved micro-PL spectra. The black dot-dashed lines show the bare cavity dispersion, $MoSe_2$ exciton emission and trion emission energies. The red solid lines show fitted upper and lower polariton modes. d) Polariton energy versus in-plane wavenumber $k_{||}$. The error bars on the energy data are 95% confidence intervals of the Gaussian fit. The error bars for the lower polariton and trion energies have been multiplied by a factor of 6 for increased visibility.

with Ω as a fitting parameter. We obtain $\hbar\Omega = 14$ meV, which satisfies the strong coupling condition (Equation (1)): 56 meV >(0.6 + 6.5) meV.

The lower energy feature shown in the PL spectrum (Figure 4c,d) around 1.62 eV is the trion–polariton emission. The trion–polariton dispersion has a negative effective mass, most likely due to the interactions between electrons, trion–polaritons, and exciton–polaritons, as described in ref. [15].

3. Conclusion

In summary, we have developed a method to reliably create high-Q microcavities for van der Waals materials and have demonstrated strong coupling in the cavity with an hBN-encapsulated monolayer of $MoSe_2$. The high-reflectance top DBR, fabricated via VTE on glass with high index contrast materials, can be readily exfoliated from the glass substrate and transferred, similar to van der Waals crystals. The cavity resonance can be controlled by hBN thickness and PMMA spin speeds. The cavity structure is one of the highest-Q DBR cavities made for vdW materials, which will facilitate future studies of nonlinear and many-body polariton phenomena.

4. Experimental Section

*Optical Characterization Measurements:*Angle-resolved reflection and PL measurements were performed using Fourier-space imaging technique with a 0.42 NA objective lens and four relay lenses. Reflection spectra were measured using a supercontinuum white light source (NKT Photonics SuperK Extreme). The supercontinuum light source had a high spatial coherence and therefore caused angle-dependent speckle patterns, which showed up at vertical stripes in the angle-resolved spectrum. The spectral resolution of reflection measurements was 0.03 nm. PL measurements were performed at 5K with the Montana Instruments Fusion 2 cryostat and a 532 nm diode laser source. Reflection and PL spectra were collected using a Princeton Instruments spectrometer.

Acknowledgements

All authors acknowledge support by the Army Research Office under Award W911NF-17-1-0312. E.P. and H.D. acknowledge support by the Air Force Office of Scientific Research under Award FA2386-21-1-4066, the National Science Foundation under Award No. DMR-2132470, the Office of Navel Research under Award N00014-21-1-2770, and the Gordon and Betty Moore Foundation under Award N031710.

Conflict of Interest

The authors declare no conflict of interest.

Data Availability Statement

The data that support the findings of this study are available from the corresponding author upon reasonable request.

Keywords

distributed Bragg reflectors, exciton–polaritons, microcavity, transition metal dichalcogenides, van der Waals materials

Received: June 22, 2022
Revised: September 8, 2022
Published online: October 31, 2022

[1] C. Weisbuch, M. Nishioka, A. Ishikawa, Y. Arakawa, *Phys. Rev. Lett.* **1992**, *69*, 3314.
[2] H. Deng, H. Haug, Y. Yamamoto, *Rev. Mod. Phys.* **2010**, *82*, 1489.

[3] T. Byrnes, N. Y. Kim, Y. Yamamoto, *Nat. Phys.* **2014**, *10*, 803.
[4] X. Liu, T. Galfsky, Z. Sun, F. Xia, E.-C. Lin, Y.-H. Lee, S. Kéna-Cohen, V. M. Menon, *Nat. Photonics* **2015**, *9*, 30.
[5] S. Dufferwiel, S. Schwarz, F. Withers, A. A. P. Trichet, F. Li, M. Sich, O. Del Pozo-Zamudio, C. Clark, A. Nalitov, D. D. Solnyshkov, G. Malpuech, K. S. Novoselov, J. M. Smith, M. S. Skolnick, D. N. Krizhanovskii, A. I. Tartakovskii, *Nat. Commun.* **2015**, *6*, 8579.
[6] N. Lundt, S. Klembt, E. Cherotchenko, S. Betzold, O. Iff, A. V. Nalitov, M. Klaas, C. P. Dietrich, A. V. Kavokin, S. Höfling, C. Schneider, *Nat. Commun.* **2016**, *7*, 13328.
[7] S. Wang, S. Li, T. Chervy, A. Shalabney, S. Azzini, E. Orgiu, J. A. Hutchison, C. Genet, P. Samorí, T. W. Ebbesen, *Nano Lett.* **2016**, *16*, 4368.
[8] L. Zhang, R. Gogna, W. Burg, E. Tutuc, H. Deng, *Nat. Commun.* **2018**, *9*, 713.
[9] N. Lundt, M. Klaas, E. Sedov, M. Waldherr, H. Knopf, M. Blei, S. Tongay, S. Klembt, T. Taniguchi, K. Watanabe, U. Schulz, A. Kavokin, S. Höfling, F. Eilenberger, C. Schneider, *Phys. Rev. B* **2019**, *100*, 121303.
[10] S. Dufferwiel, T. P. Lyons, D. D. Solnyshkov, A. A. P. Trichet, F. Withers, S. Schwarz, G. Malpuech, J. M. Smith, K. S. Novoselov, M. S. Skolnick, D. N. Krizhanovskii, A. I. Tartakovskii, *Nat. Photonics* **2017**, *11*, 497.
[11] N. Lundt, Ł. Dusanowski, E. Sedov, P. Stepanov, M. M. Glazov, S. Klembt, M. Klaas, J. Beierlein, Y. Qin, S. Tongay, M. Richard, A. V. Kavokin, S. Höfling, C. Schneider, *Nat. Nanotechnol.* **2019**, *14*, 770.
[12] C. Rupprecht, N. Lundt, M. Wurdack, P. Stepanov, E. Estrecho, M. Richard, E. A. Ostrovskaya, S. Höfling, C. Schneider, *Appl. Phys. Lett.* **2021**, *118*, 103103.
[13] G. Kedawat, S. Srivastava, V. K. Jain, P. Kumar, V. Kataria, Y. Agrawal, B. K. Gupta, Y. K. Vijay, *ACS Appl. Mater. Interfaces* **2013**, *5*, 4872.
[14] Y. Qu, S. Hou, S. R. Forrest, *ACS Photonics* **2020**, *7*, 867.
[15] S. Dhara, C. Chakraborty, K. M. Goodfellow, L. Qiu, T. A. O'Loughlin, G. W. Wicks, S. Bhattacharjee, A. N. Vamivakas, *Nat. Phys.* **2018**, *14*, 130.